

Supplementary Information

Eu^{2+} Luminescence in CaYGaO_4 Olivine: A New Efficient Red Phosphor for Warm Illumination

Tao Hu^{*#}, Zelong Jiang[#], Bo Wang, Ting Yu, Dawei Wen*, Qinguang Zeng, and Yan Gao*

Tao Hu^{*#a}, Zelong Jiang^{#a}, Bo Wang^a, Ting Yu^a, Dawei Wen^{*a}, Qinguang Zeng^a, and Yan Gao^{*a}

^a*School of Applied Physics and Materials, Wuyi University, Jiangmen 529020, Guangdong Province, P. R. China*

Corresponding Authors

* hutaowyu@sina.com (T. Hu)

* ontaiii@163.com (D. W. Wen)

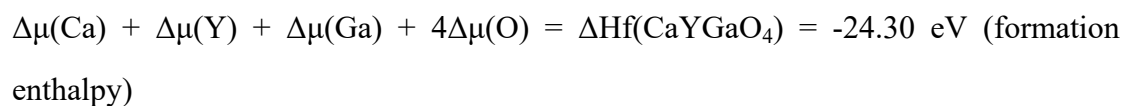
* gaoyan_chn@sina.com (Y. Gao)

DFT calculations: The DFT calculations were performed using the Vienna Ab initio Simulation Package (VASP) v6.20.¹ The $4s^24p^64d^25s^1$, $3p^64s^2$, $3d^{10}4s^24p^1$, $2s^22p^4$ and $4f^75s^25p^66s^2$ electrons of Y, Ca, Ga, O and Eu atoms, respectively, were treated as valence electrons, and an additional Hubbard U term of 2.5 eV was set for the 4f states of the Eu atoms.²⁻⁴ The crystal structures were optimized using the quasi-Newton algorithm with a convergence criterion of 2×10^{-2} eV/Å². A $1 \times 1 \times 1$ unit cell was used as the calculation model with $3 \times 4 \times 3$ K-points, where the energy convergence criteria were set to 1×10^{-8} eV using PBEsol functionnal. The defect formation energies were calculated by the following equation:⁵

$$\Delta H = E_D - E_H + \sum_i n_i \mu_i + qE_F + E_{corr}$$

where ΔH is the formation energy, E_D is the total energy of the defect cell, E_H is the total energy of host lattice, μ_i is the chemical potential for the element, the chemical potentials of Ca, Y and Eu were approximated by the energy of the corresponding metallic atom due to the reducing atmosphere in the synthesis process ($\Delta\mu(\text{Ca}) = -2.1199$ eV/atom; $\Delta\mu(\text{Y}) = -6.8195$ eV/atom; -1.1497 eV/atom).⁶ qE_F is the electron chemical potential and E_{corr} is the finite size corrections.⁷⁻⁹

Formation enthalpy was calculated according to the total energy of the unit cell and fitted elemental-phase reference energies:¹⁰



According to the above equations, we obtain:

$\Delta\mu(\text{O}) \in [-6.075, 0] \text{ eV}$ (-6.075 eV for extremely oxygen-poor and 0 for oxygen-rich conditions, respectively)

$\Delta\mu(\text{Ca}) \in (-24.30, -0.515] \text{ eV}$

$\Delta\mu(Y) \in (-24.30, -0.7575]$ eV

$\Delta\mu(Ga) \in (-24.30, 0]$ eV

$\Delta\mu(Eu) \in (-\infty, -6.8225]$ eV

The chemical potentials depend on the chemical potential of the related compounds

$\Delta\mu(CaO)$, $\Delta\mu(Y_2O_3)$, $\Delta\mu(Y_2O_3)$ and $\Delta\mu(Eu_2O_3)$ according to reference R7:

$$\Delta\mu(Ca) = \Delta Hf(CaO) - \Delta\mu(O) + \Delta\mu(CaO)$$

$$\Delta\mu(Y) = 0.5\Delta Hf(Y_2O_3) - 1.5\Delta\mu(O) + 0.5\Delta\mu(Y_2O_3)$$

$$\Delta\mu(Eu) = 0.5\Delta Hf(Eu_2O_3) - 1.5\Delta\mu(O) + 0.5\Delta\mu(Eu_2O_3)$$

$$\Delta\mu(Ga) = 0.5\Delta Hf(Ga_2O_3) - 1.5\Delta\mu(O) + 0.5\Delta\mu(Ga_2O_3)$$

The formation energy E_f of $Eu^{2+/3+}$ in Y sites was independent on the synthesis atmosphere because E_f is a function of $\Delta\mu(Y) - \Delta\mu(Eu)$. Here, $\Delta\mu(Y) - \Delta\mu(Eu) = 0.5\Delta Hf(Y_2O_3) - 0.5\Delta Hf(Eu_2O_3) + 0.5\Delta\mu(Y_2O_3) - 0.5\Delta\mu(Eu_2O_3)$. However, E_f for Eu substituting Ca is a function of $\Delta\mu(Y) - \Delta\mu(Eu)$. Here, $\Delta\mu(Ca) - \Delta\mu(Eu) = \Delta Hf(CaO) - 0.5\Delta Hf(Eu_2O_3) + \Delta\mu(CaO) - 0.5\Delta\mu(Eu_2O_3) + 0.5\Delta\mu(O)$. Therefore, the oxygen-rich environment is not beneficial to the $Eu^{2+/3+}$ substituting Ca sites.

Furthermore, excess of CaO ($CaCO_3$) raw material is beneficial to the $Eu^{2+/3+}$ occupying Y sites while excess of Y_2O_3 is beneficial to $Eu^{2+/3+}$ occupying Ca sites, respectively.

The bandgap and density of states calculation were performed in WIEN2K code using PBE-GGA and Modified Becke-Johnson potential (MBJ) method based on the optimized structure.

1 G. Kresse, J. Furthmüller, *Phys. Rev. B.*, 1996, **54**, 11169.

2 J. Qiao, L. Ning, M. S. Molokeev, Y. C. Chuang, Q. Liu, Z. Xia, *J. Am. Chem. Soc.*, 2018, **140**, 9730.

3 A. Chaudhry, R. Bouthko, S. Chourou, G. Zhang, N. Grønbech-Jensen, A. Canning, *Phys. Rev. B: Condens. Matter Mater. Phys.*, 2014, **89**, 155105.

4 M. Amachraa, S. Li, P.-Y. Huang, R.-S. Liu, Z. Wang, R.-J. Xie, S.P. Ong, *Chem. Mater.*, 2022, **34**, 4039.

- 5 A. Goyal, P. Gorai, H. Peng, S. Lany, V. Stevanović, *Comput. Mater. Sci.*, 2017, **130**, 1.
- 6 X. Huang, Z. Qiao, J. Wen, L. Ning, *J. Phys. Chem. C*, 2020, **124**, 13400-13408.
- 7 P. Blaha, K. Schwarz, F. Tran, R. Laskowski, G. K. Madsen, L. D. Marks, *J. Chem. Phys.*, 2020, **152**, 074101.
- 8 F. Tran, P. Blaha, *Phys. Rev. Lett.*, 2009, **102**, 226401.
- 9 D. Koller, F. Tran, P. Blaha, *Phys. Rev. B.*, 2012, **85**, 155109.
- 10 V. Stevanović, S. Lany, X. Zhang, A. Zunger, *Phys. Rev. B.*, 2012, **85**, 115104.

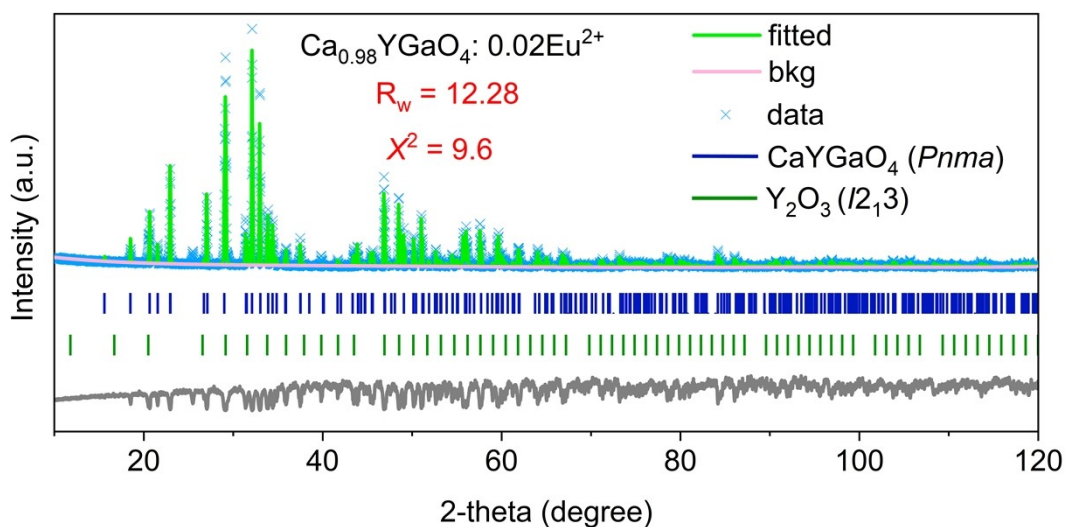


Fig. S1 Rietveld refinement on the XRD data of Ca_{0.98}YGaO₄:0.02Eu²⁺ red phosphor.

Table S1 The Refined structural parameters of $\text{Ca}_{0.98}\text{YGaO}_4:0.02\text{Eu}^{2+}$ phosphor

Atom	x	y	z	Wycoff position	Occ.	
Ca	0.50000	0.50000	0.50000	4a	1.0000	symmetry : orthorhombic
Y	0.27770	0.75000	-0.00260	4c	1.0000	space group : Pnma(62)
Ga	0.59700	0.75000	0.05890	4c	1.0000	$a = 11.34378 \text{ \AA}$
O1	0.60000	0.75000	-0.28300	8d	1.0000	$b = 6.59648 \text{ \AA}$
O2	0.66960	0.53190	0.22880	4c	1.0000	$c = 5.28819 \text{ \AA}$
O3	0.44810	0.75000	0.20900	4c	1.0000	$V = 395.710 \text{ \AA}^3$

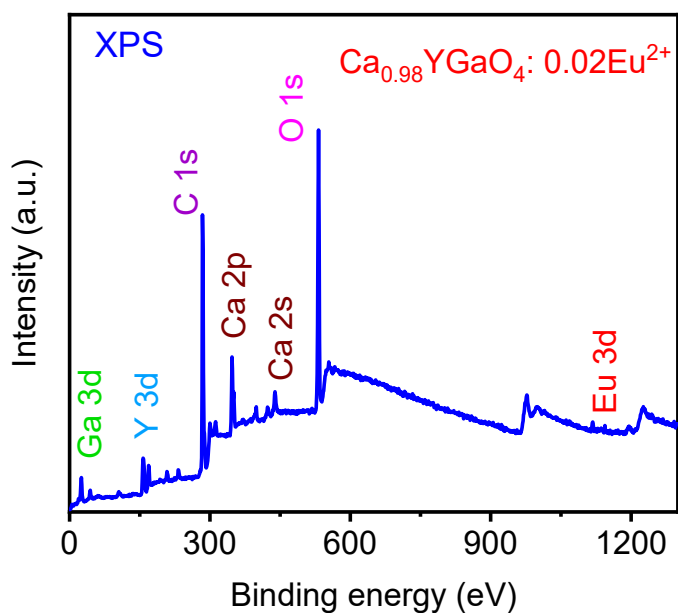


Fig. S2 XPS wide scan spectra of $\text{Ca}_{0.98}\text{YGaO}_4:0.02\text{Eu}^{2+}$ red phosphor,

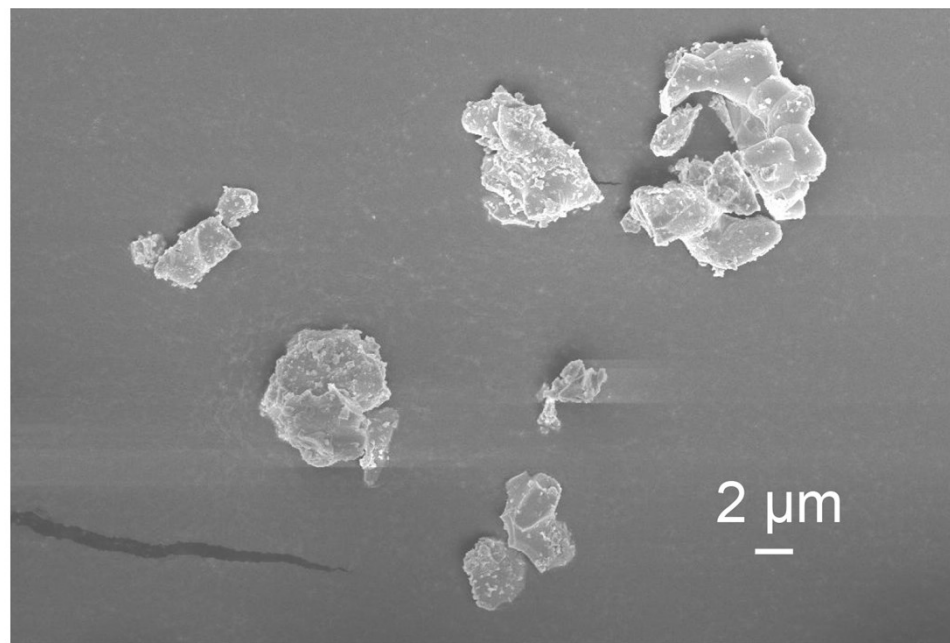


Fig. S3 SEM image of $\text{Ca}_{0.98}\text{YGaO}_4:0.02\text{Eu}^{2+}$ red phosphor.

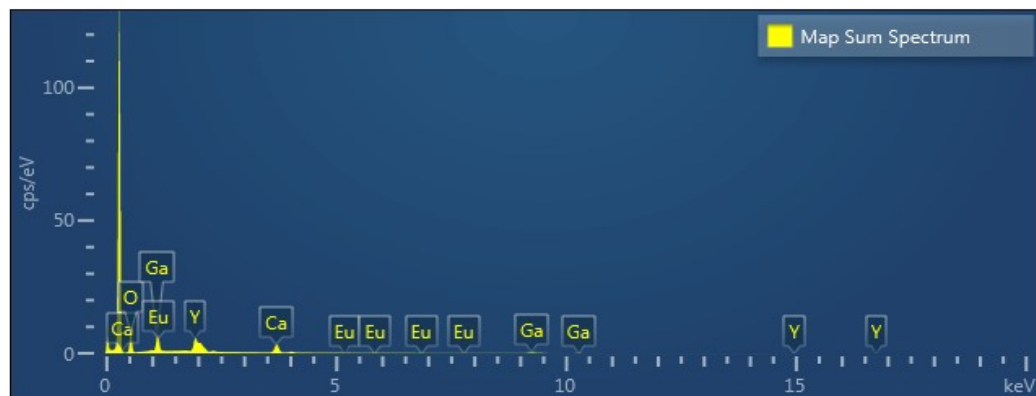


Fig. S4 Energy dispersive X-ray (EDX) spectrum of the pristine $\text{Ca}_{0.98}\text{YGaO}_4:0.02\text{Eu}^{2+}$ red phosphor.

Tab. S2 Element analysis of the pristine $\text{Ca}_{0.98}\text{YGaO}_4:0.02\text{Eu}^{2+}$ by Energy dispersive X-ray (EDX) spectrum.

Element	Line Type	k Ratio	Wt%	Wt% Sigma	Atomic %
O	K series	0.02820	39.03	0.12	72.32
Ca	K series	0.03407	13.64	0.06	10.09
Ga	L series	0.03377	21.64	0.09	9.20
Y	L series	0.04768	24.44	0.13	8.15
Eu	L series	0.00245	1.25	0.13	0.24
Total:			100.00		100.00

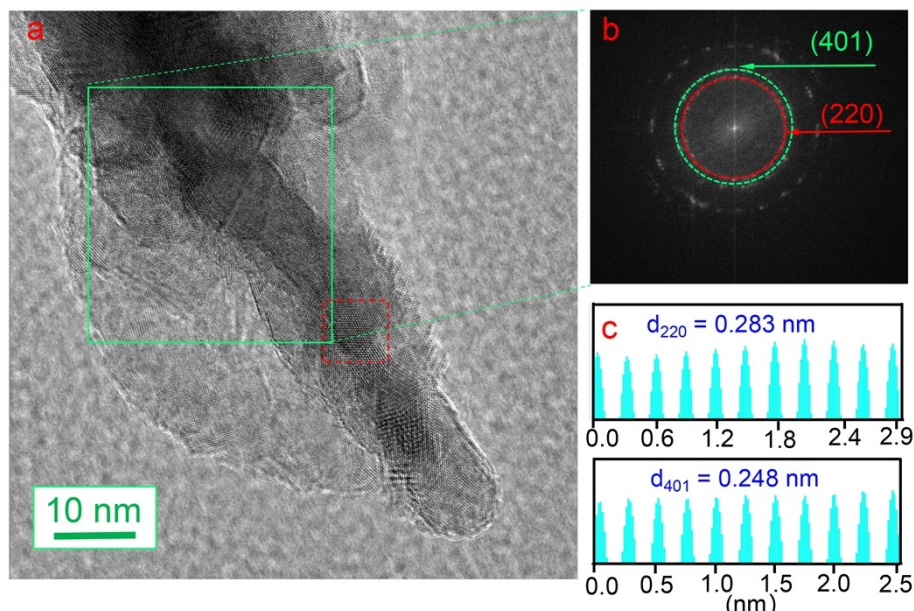


Fig. S5 (a) HRTEM observations of the $\text{Ca}_{0.98}\text{YGaO}_4:0.02\text{Eu}^{2+}$ phosphor, (b) FFT images of the denoted green rectangular regions in figure a. (c) Intensity profile obtained by drawing the straight-line perpendicular to the (220) and (401) planes.

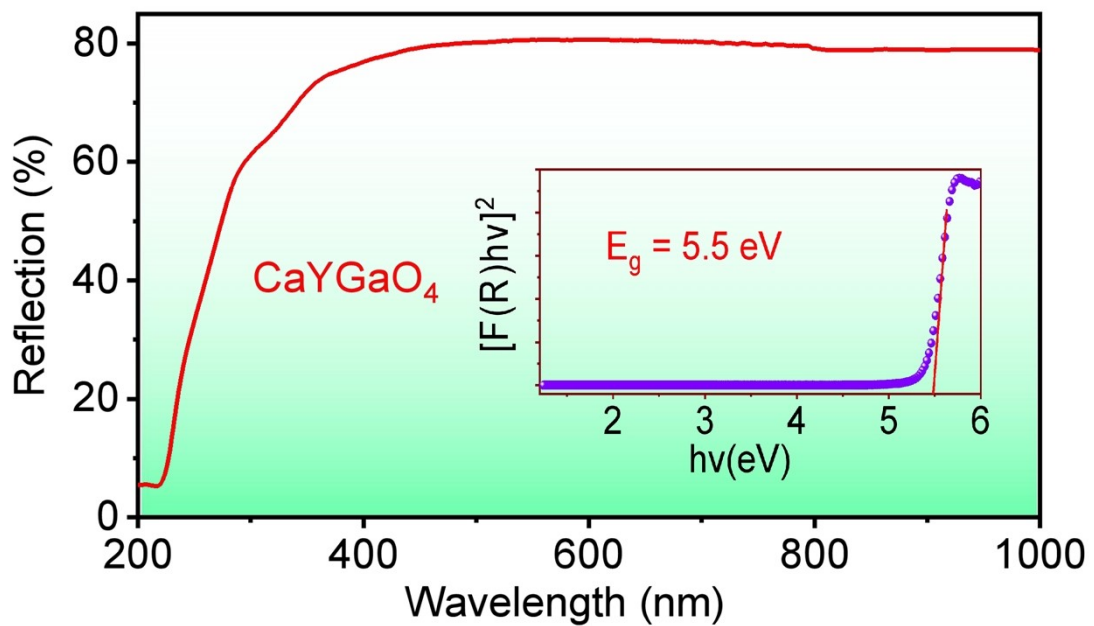


Fig. S6 Diffuse reflectance spectra of CaYGaO_4 host. The inset is Kubelka-Munk transformed diffuse reflectance spectra for determination of the host bandgap (E_g) by plotting $[F(R)hv]^2$ versus photon energy $h\nu$, where R is the reflectance, and $F(R)$ is the Kubelka-Munk function ($F(R)=(1-R)^2/2R$).

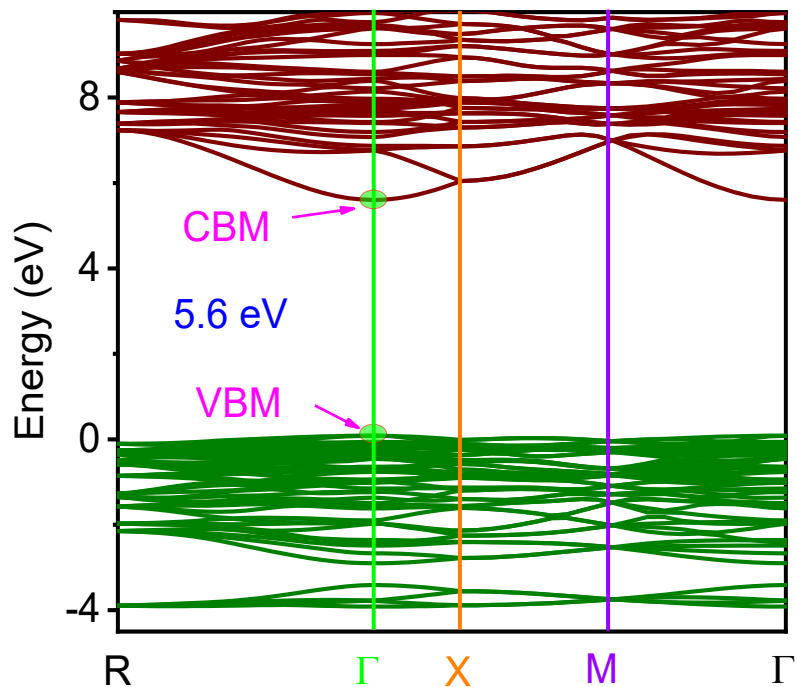


Fig. S7 The calculated energy band structure of CaYGaO_4 host.

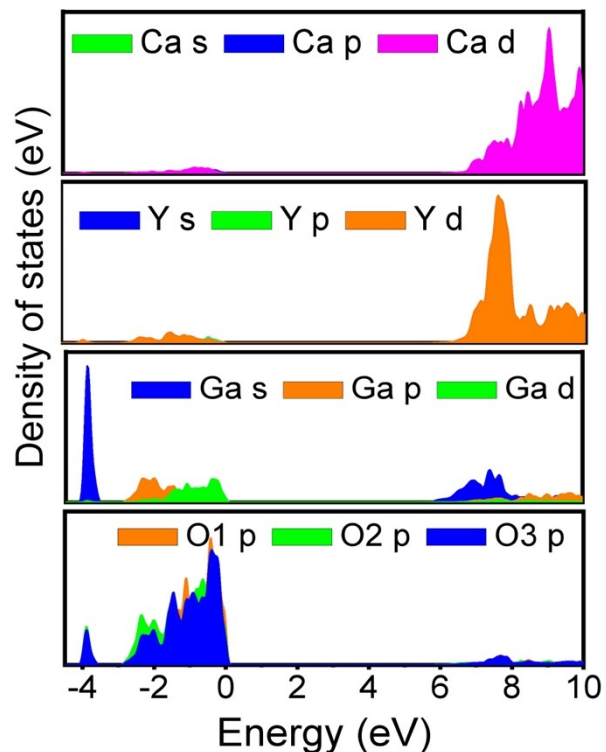


Fig. S8 the partial (Ca, Y, Ga and O atom) density state of CaYGaO_4 host.

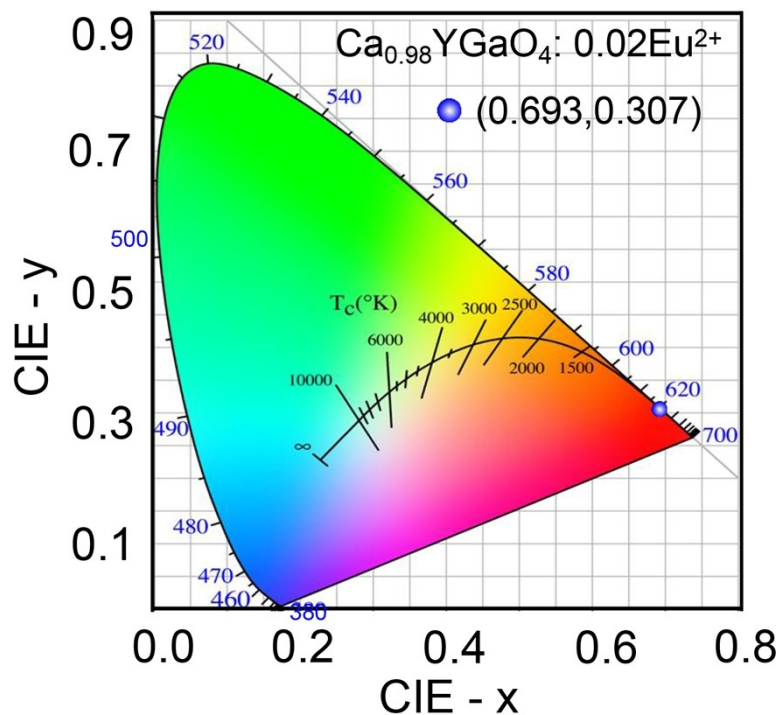


Fig. S9 The CIE coordinate of $\text{CaYGaO}_4:\text{Eu}^{2+}$.

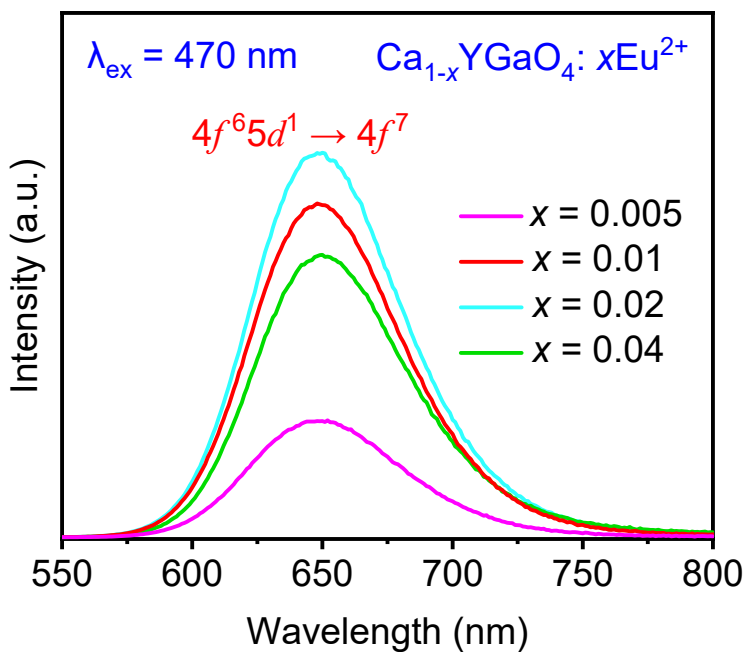


Fig. S10 PL spectra of $\text{Ca}_{1-x}\text{YGaO}_4:\text{xEu}^{2+}$ ($x = 0.005\text{--}0.04$) samples under 470 nm blue light excitation.

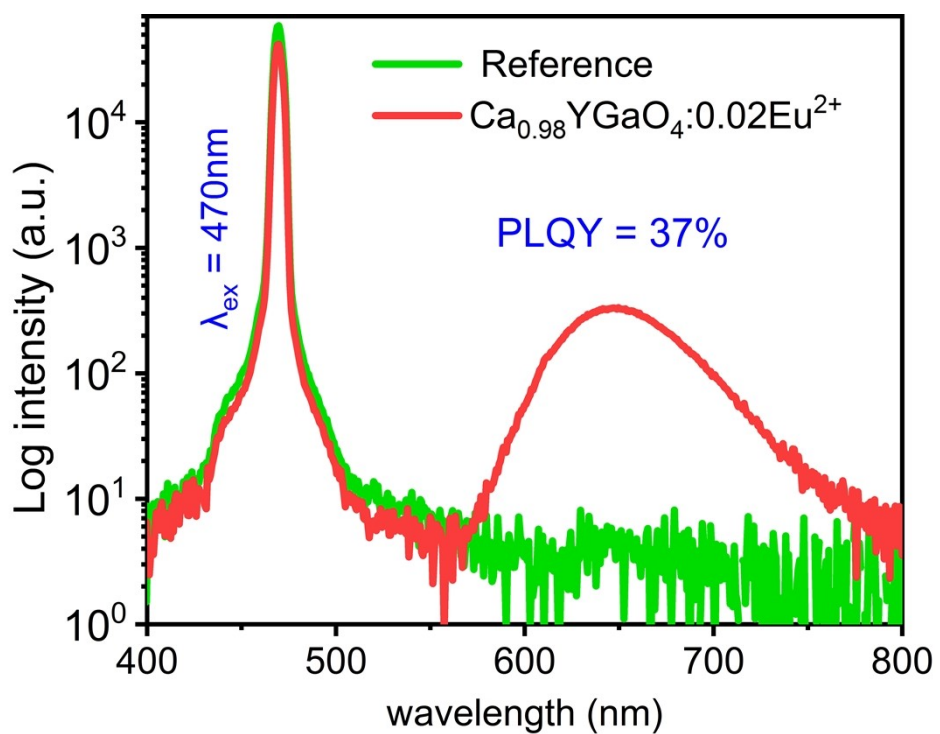


Fig. S11 The PLQY of $\text{Ca}_{0.98}\text{YGaO}_4:0.02\text{Eu}^{2+}$ red phosphor.

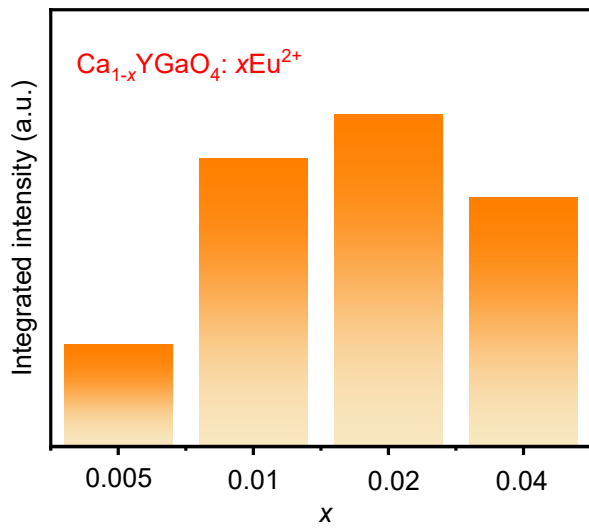


Fig. S12 Integrated PL intensity of $\text{Ca}_{1-x}\text{YGaO}_4:xE\text{u}^{2+}$ ($x = 0.005\text{--}0.04$) samples under 470 nm blue light excitation.

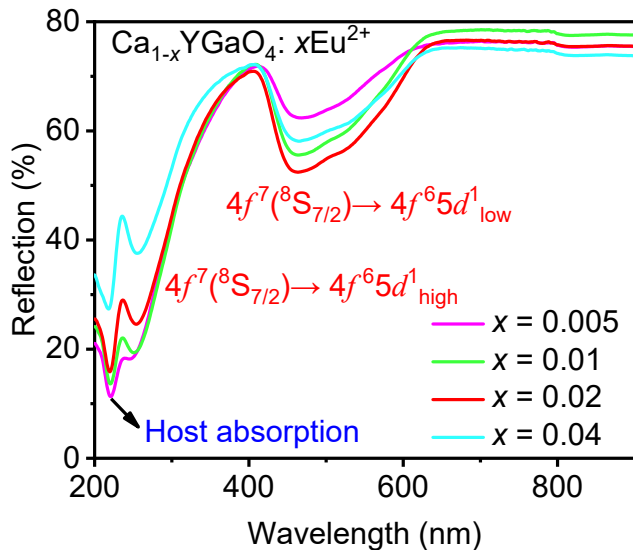


Fig. S13 Diffuse reflectance spectra of $\text{Ca}_{1-x}\text{YGaO}_4:xE\text{u}^{2+}$ ($x = 0.005\text{--}0.04$).

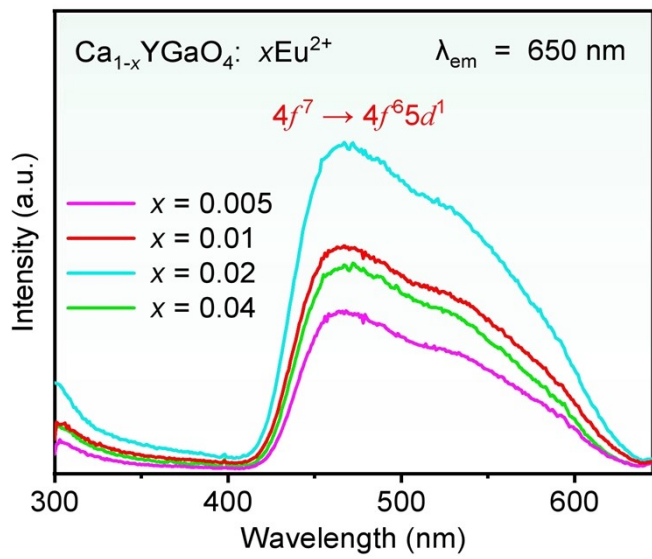


Fig. S14 PLE spectra ($\lambda_{\text{em}} = 650 \text{ nm}$) of Ca_{1-x}YGaO₄:xEu²⁺ ($x = 0.005\text{--}0.04$).

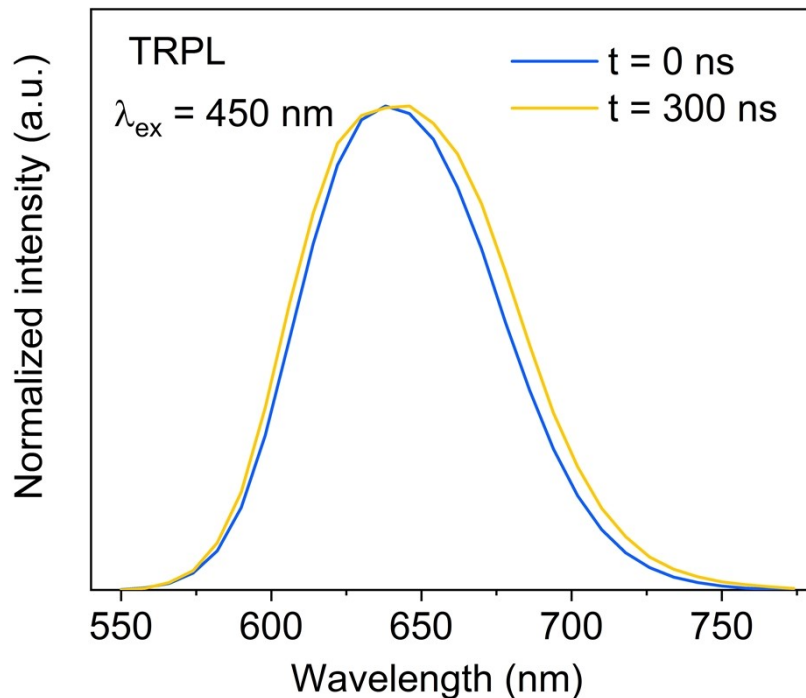


Fig. S15 The normalized transient PL spectra of Ca_{0.98}YGaO₄:0.02Eu²⁺ phosphor at time of 0 ns and 300 ns

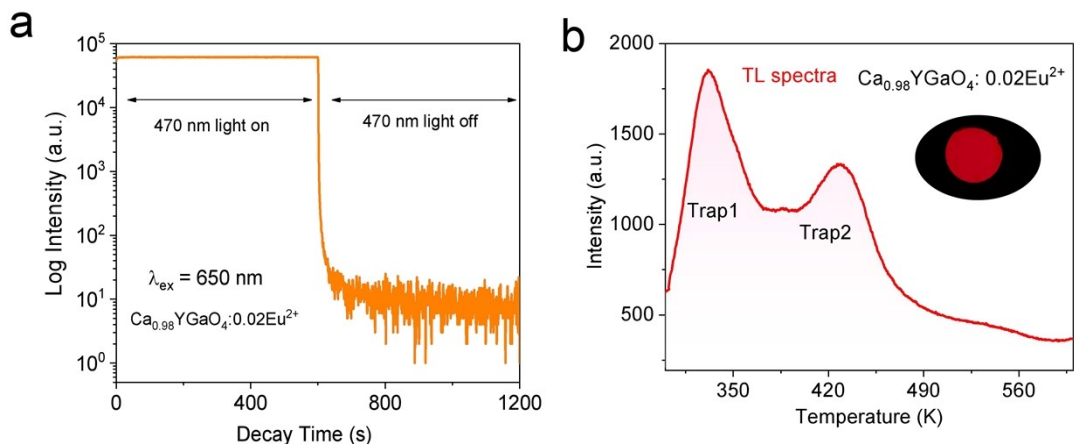


Fig. S16 (a) Persistent luminescence decay curve, and (b) TL spectra of $\text{Ca}_{0.98}\text{YGaO}_4: 0.02\text{Eu}^{2+}$ phosphor, the inset show the image of the phosphor taken after stopping blue light irradiation.

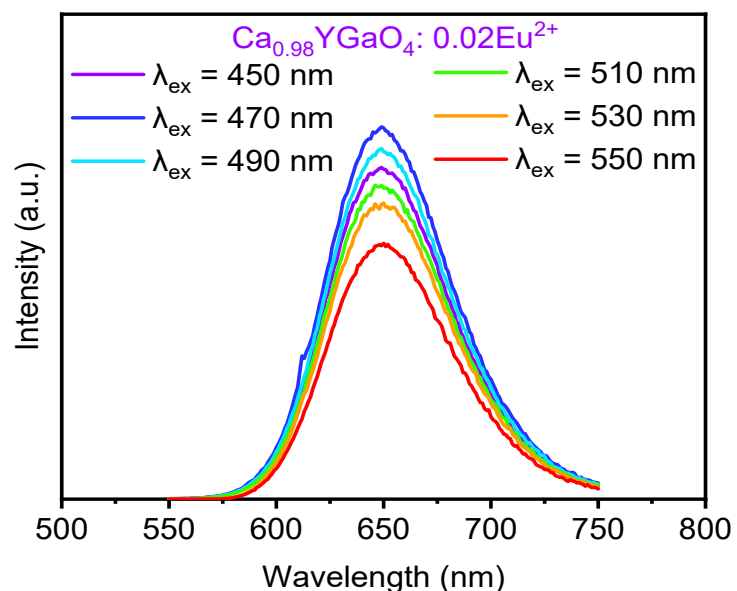


Fig. S17 The site-selective PL spectra of $\text{Ca}_{0.98}\text{YGaO}_4: 0.02\text{Eu}^{2+}$ phosphor at excitation of 450–550 nm light.

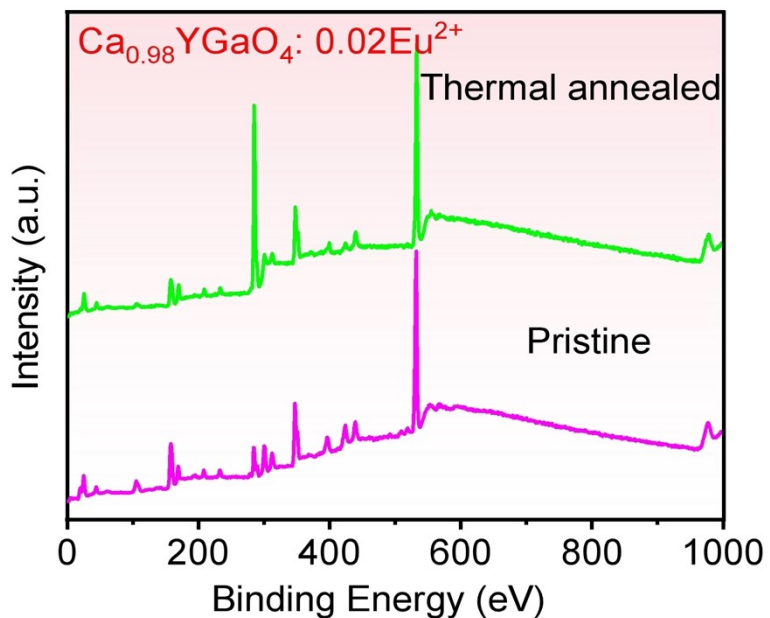


Fig. S18 XPS survey scan of the pristine and thermal annealed $\text{Ca}_{0.98}\text{YGaO}_4:0.02\text{Eu}^{2+}$ red phosphor.

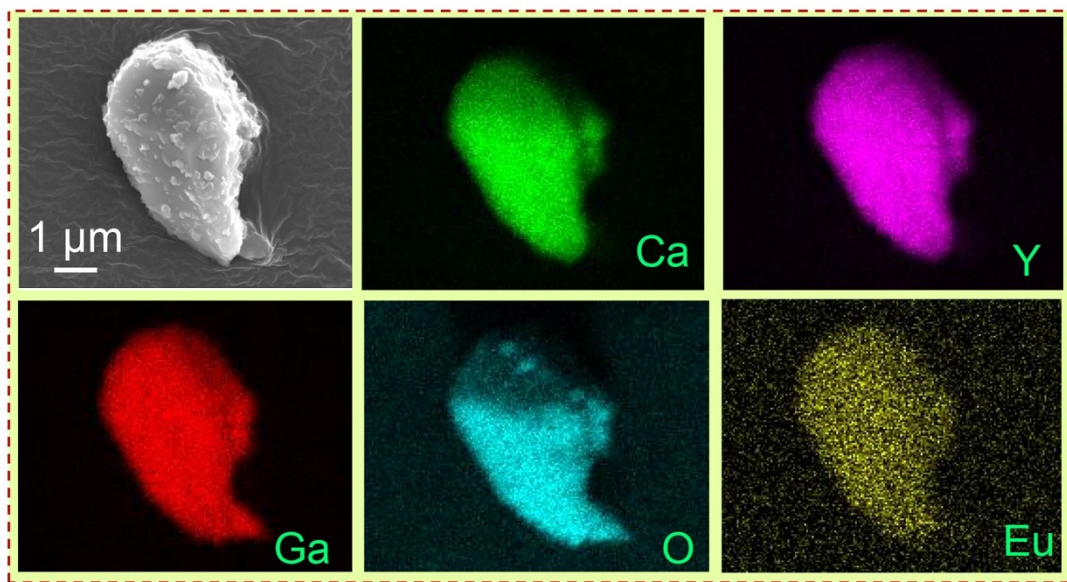


Fig. S19 EDX elemental mappings of thermally annealed $\text{Ca}_{0.98}\text{YGaO}_4:0.02\text{Eu}^{2+}$ red phosphor.

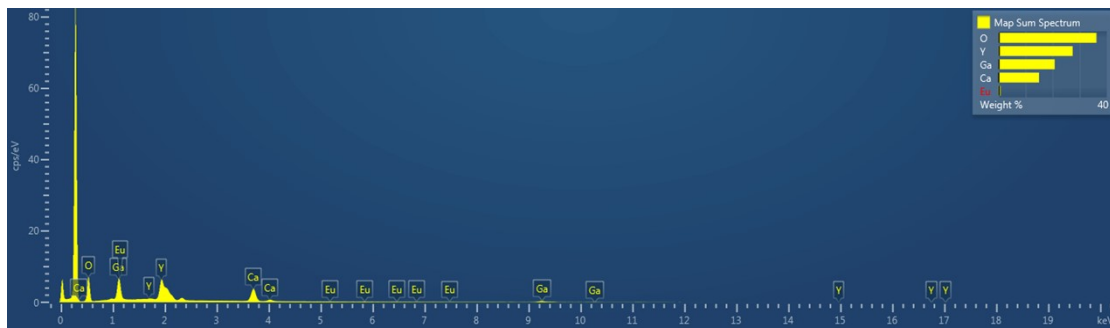


Fig. S20 Energy dispersive X-ray (EDX) spectrum of the thermal annealed $\text{Ca}_{0.98}\text{YGaO}_4:0.02\text{Eu}^{2+}$ red phosphor.

Tab. S3 Element analysis of the thermal annealed $\text{Ca}_{0.98}\text{YGaO}_4:0.02\text{Eu}^{2+}$ by Energy dispersive X-ray (EDX) spectrum.

Element	Line Type	k Ratio	Wt%	Wt% Sigma	Atomic %
O	K series	0.02542	36.17	0.24	69.68
Ca	K series	0.03880	14.95	0.13	11.50
Ga	L series	0.03372	20.75	0.18	9.17
Y	L series	0.05634	27.39	0.26	9.50
Eu	L series	0.00153	0.75	0.26	0.15
Total:			100.00		100.00

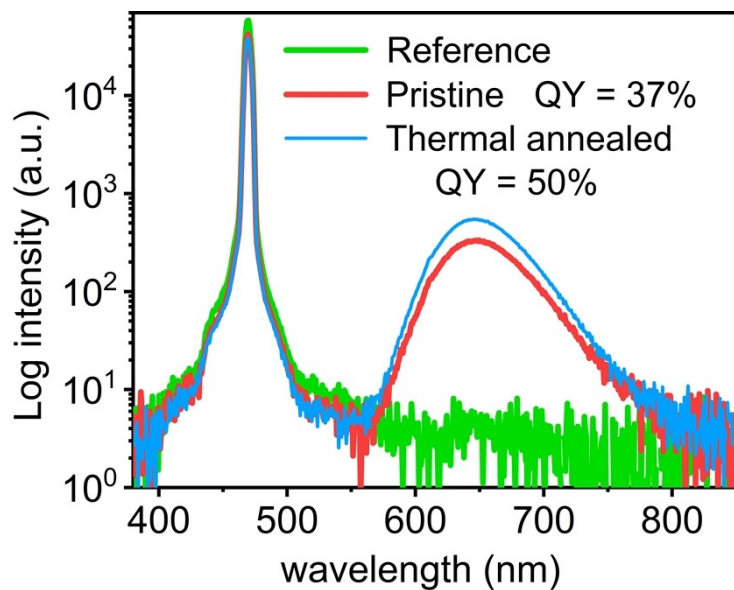


Fig. S21 The PLQY of the pristine and thermal annealed $\text{Ca}_{0.98}\text{YGaO}_4:0.02\text{Eu}^{2+}$ red phosphor.

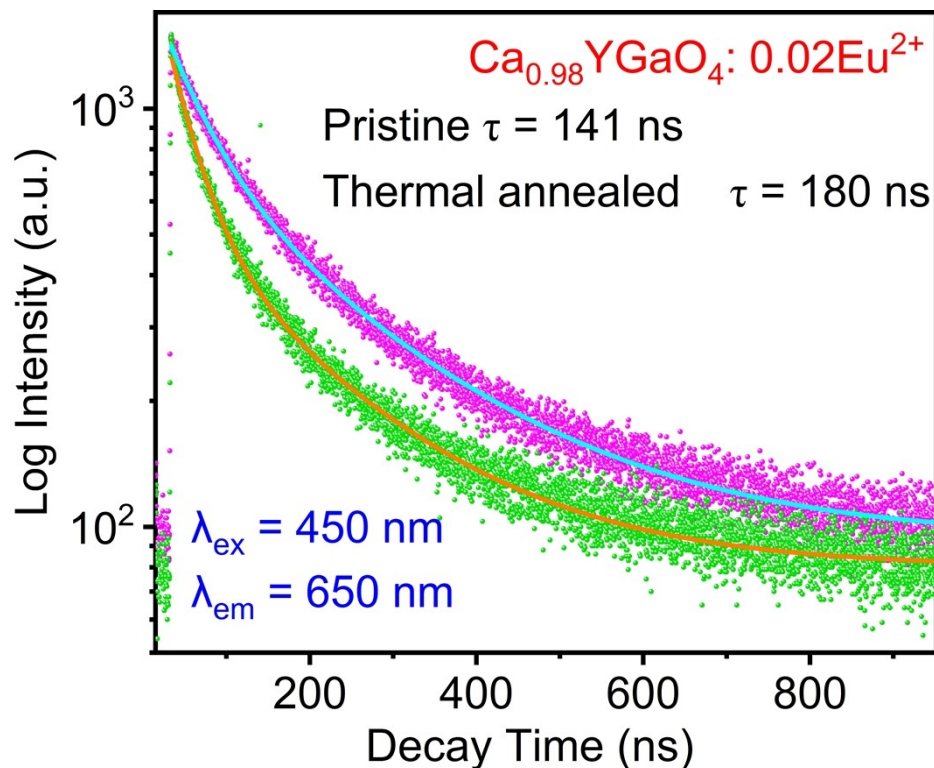


Fig. S22 PL decay curves of the pristine and thermal annealed $\text{Ca}_{0.98}\text{YGaO}_4:0.02\text{Eu}^{2+}$ phosphor by monitoring the emission at 650 nm. The value of the vertical axis for the PL decay curves isn't starts at zero. This is because the phosphor has weak persistent

luminescence at 650 nm, which raises the decay curve overall.

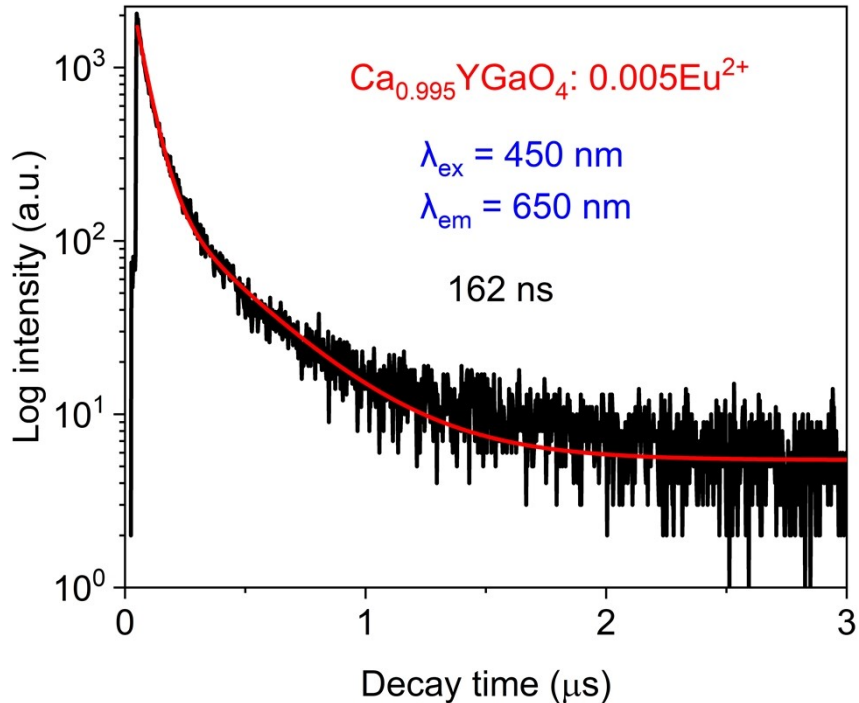


Fig. S23 PL decay curve of the pristine $\text{Ca}_{0.995}\text{YGaO}_4:0.005\text{Eu}^{2+}$ phosphor by monitoring the emission at 650 nm.

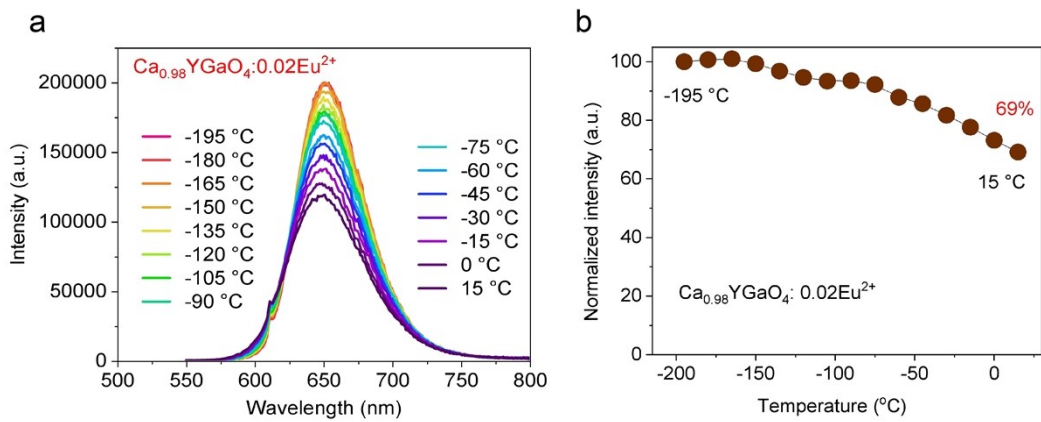


Fig. S24 (a) Temperature-dependent PL spectra of thermal annealed $\text{Ca}_{0.98}\text{YGaO}_4:0.02\text{Eu}^{2+}$ phosphor in the temperature range -195 °C to 15 °C, (b) Normalized integrated PL intensity.

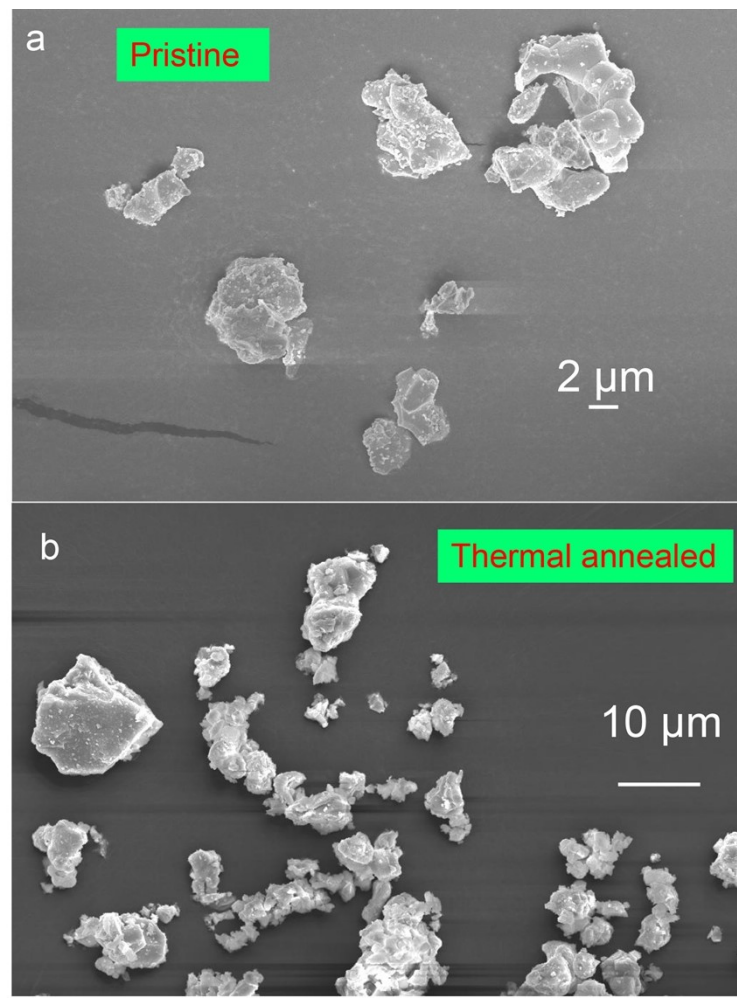


Fig. S25 SEM image of the pristine and thermal annealed $\text{Ca}_{0.98}\text{YGaO}_4:0.02\text{Eu}^{2+}$ red phosphor.

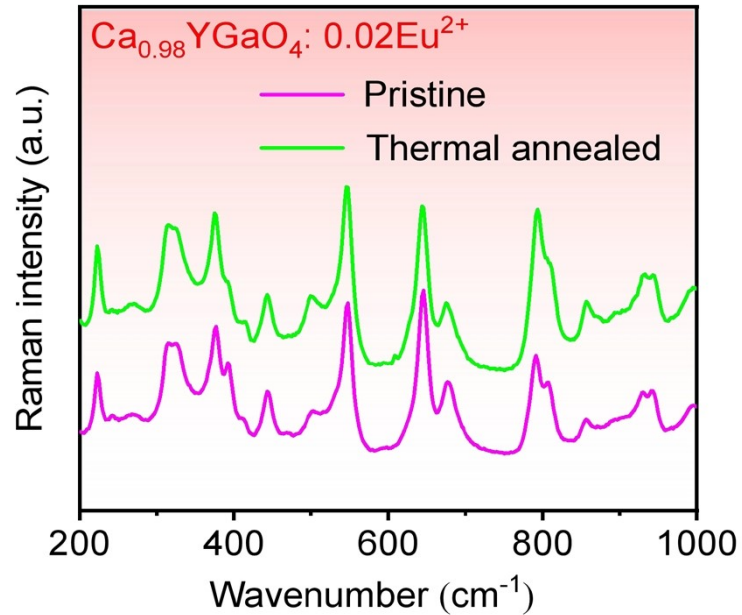


Fig. S26 Raman spectra of the pristine and thermal annealed $\text{Ca}_{0.98}\text{YGaO}_4: 0.02\text{Eu}^{2+}$ red phosphor.

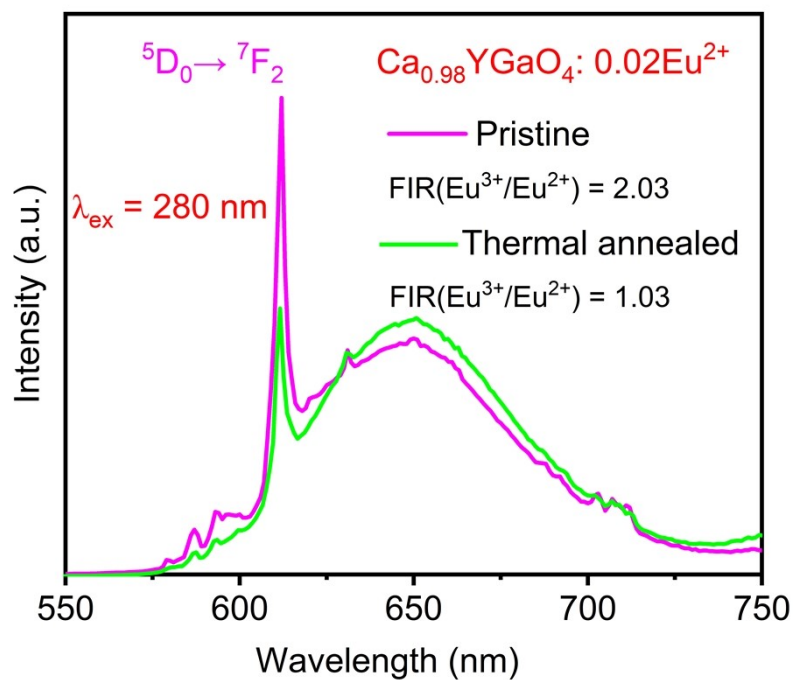


Fig. S27 The PL spectra of the pristine and thermal annealed phosphor excited at $\text{Eu}^{3+}-\text{O}^{2-}$ charge transfer band.

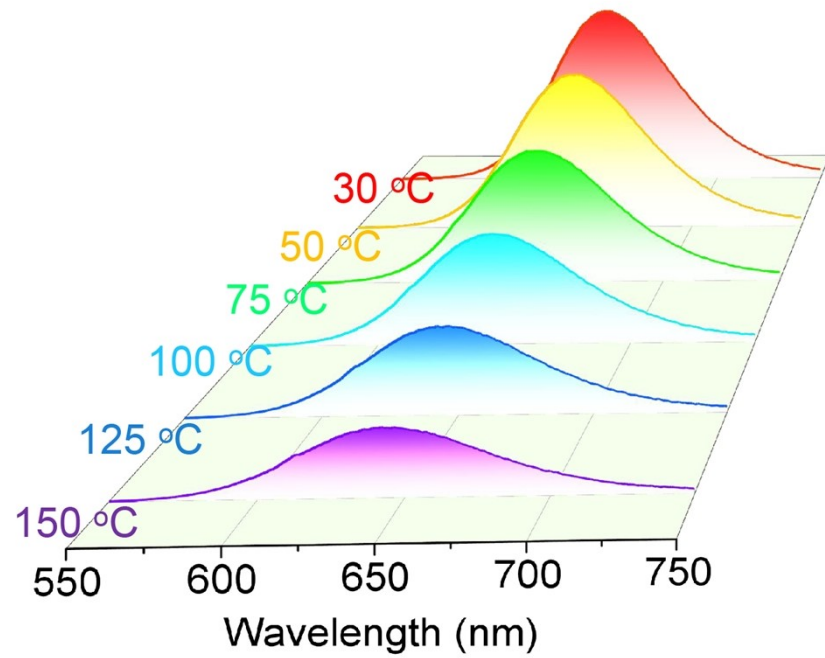


Fig. S28 Temperature dependent PL spectra of pristine $\text{Ca}_{0.98}\text{YGaO}_4:0.02\text{Eu}^{2+}$ phosphor in the temperature range of room temperature to 150°C.

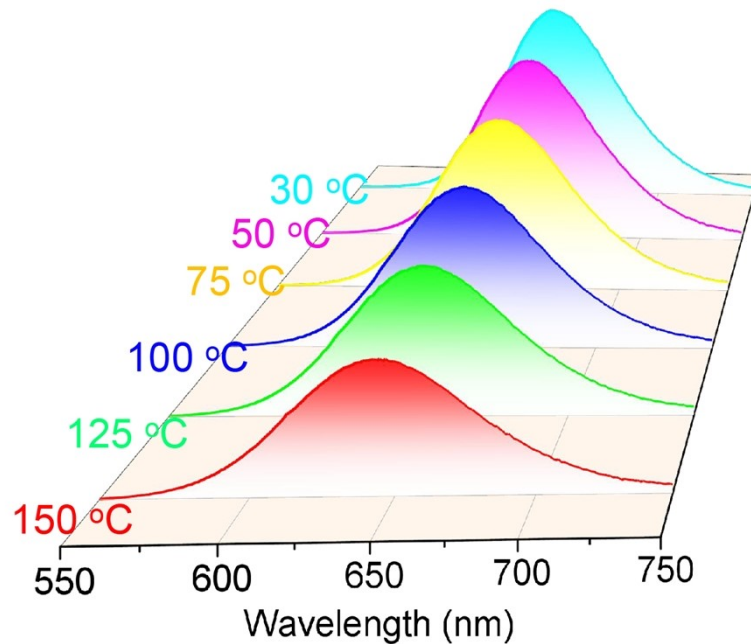


Fig. S29 Temperature dependent PL spectra of thermally annealed $\text{Ca}_{0.98}\text{YGaO}_4:0.02\text{Eu}^{2+}$ phosphor in the temperature range of room temperature to 150°C.

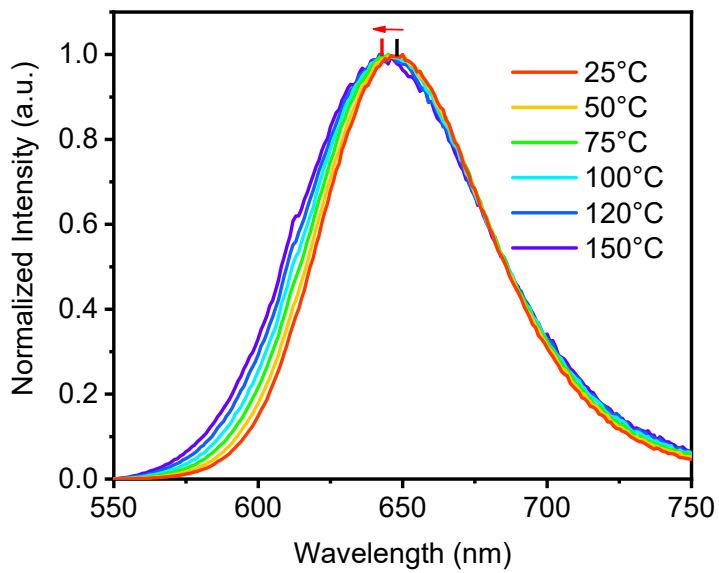


Fig. S30 Normalized Temperature dependent PL spectra of thermally annealed $\text{Ca}_{0.98}\text{YGaO}_4:0.02\text{Eu}^{2+}$ phosphor in the temperature range of room temperature to 150°C.

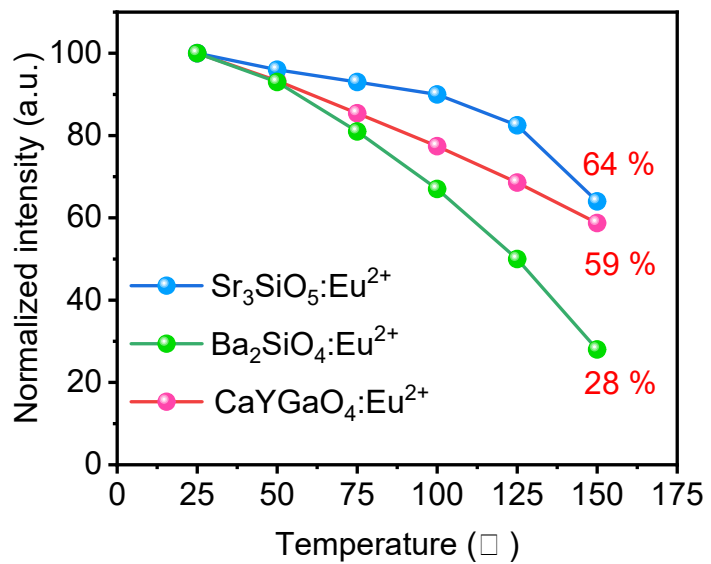


Fig. S31 Comparison of the anti-thermal quenching property of $\text{CaYGaO}_4:\text{Eu}^{2+}$, $\text{Ba}_2\text{SiO}_4:\text{Eu}^{2+}$, $\text{Sr}_3\text{SiO}_5:\text{Eu}^{2+}$ phosphor.

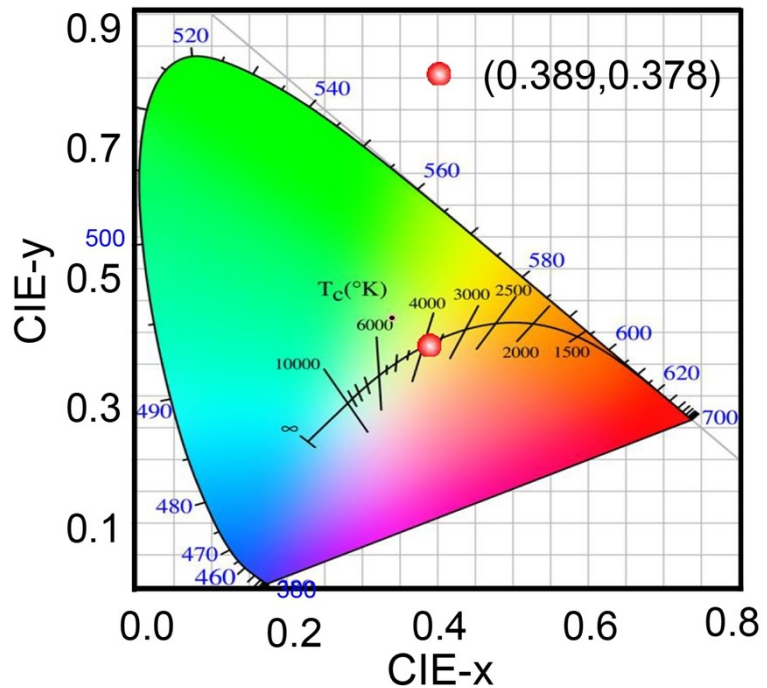


Fig. S32 The CIE coordinate of the LED fabricated by coating commercial YAG:Ce³⁺ yellow phosphor and the as-developed Ca_{0.98}YGaO₄:0.02Eu²⁺ red phosphor on a 450 nm LED chip.